Journal Pre-proof

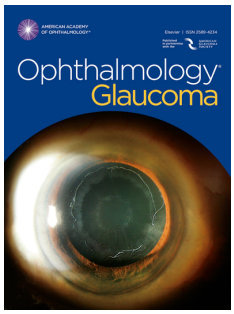

Glaucoma Rose Plot Analysis: Detecting Early Structural Progression Using Angular Histograms

Timothy E. Yap, Benjamin M. Davis, Philip A. Bloom, M. Francesca Cordeiro, Eduardo M. Normando

PII: S2589-4196(22)00095-3

DOI: https://doi.org/10.1016/j.ogla.2022.06.002

Reference: OGLA 423

To appear in: *OPHTHALMOLOGY GLAUCOMA*

Received Date: 11 February 2022

Revised Date: 26 May 2022

Accepted Date: 1 June 2022

Please cite this article as: Yap TE, Davis BM, Bloom PA, Cordeiro MF, Normando EM, Glaucoma Rose Plot Analysis: Detecting Early Structural Progression Using Angular Histograms, *OPHTHALMOLOGY GLAUCOMA* (2022), doi: https://doi.org/10.1016/j.ogla.2022.06.002.

Glaucoma Rose Plot Analysis: Detecting Early Structural Progression Using Angular Histograms

Timothy E. Yap[1,2], Benjamin M. Davis[3,4], Philip A. Bloom[1,2], M. Francesca Cordeiro[1,2,4], Eduardo M. Normando[1,2,*]

[1] Western Eye Hospital, Imperial College Healthcare NHS Trust (ICHNT), London, NW1 5QH, UK
[2] Imperial College Ophthalmic Research Group (ICORG), Imperial College London, NW1 5QH, UK
[3] Central Laser Facility, Rutherford Appleton Laboratory, Oxfordshire. OX11 0QX, UK.
[4] Glaucoma and Retinal Neurodegeneration Group, Department of Visual Neuroscience, UCL Institute of Ophthalmology, London EC1V 9EL, UK

* Correspondence: Dr. E. M. Normando, Western Eye Hospital, 153-173 Marylebone Rd, Marylebone, London NW1 5QH. E-mail: e.normando@nhs.net

Authors:

1. Timothy E. Yap MBChB MA MRCP
2. Benjamin Davis, PhD
3. Philip A. Bloom, FRCOphth
4. M. Francesca Cordeiro, PhD MRCP FRCOphth
5. Eduardo M. Normando, MD PhD FEBO

Site of Study:

Western Eye Hospital, Imperial College Healthcare NHS Trust, London, UK

Grants and Funds:

None

Conflict of Interest:

MFC has received speaker's fees and contribution in kind from Heidelberg Engineering.

Meeting presentation:

Data contained in this manuscript has been submitted for consideration for poster presentation at ARVO Denver, May 1-4 2022.

Address for reprints:

Dr. Eduardo Normando
Imperial College Ophthalmology Research Group (ICORG)
Western Eye Hospital
153-173 Marylebone Rd
London
NW1 5QH
UK
e.normando@nhs.net

Taxonomy topics / keywords:

Glaucoma, optical coherence tomography, retinal imaging, retinal nerve fibre layer, progression analysis, angular histograms, rose plot.

Running head

Glaucoma Rose Plot Analysis

Abstract

Purpose

To evaluate novel 'Rose Plot Analysis' (RPA) in the analysis and presentation of glaucoma structural progression data.

Design

A case-control image analysis study using retrospective retinal imaging series

Subjects

Subjects with open-angle glaucoma, with at least five registered spectral-domain optical coherence tomography (SD-OCT) scans.

Methods

Glaucoma RPA analysis was developed combining a novel application of angular histograms and dynamic cluster analysis of circumpapillary RNFL (cRNFL) OCT data. RPA plots were created for each eye and for each visit. Significant clusters of progression were indicated in red. Three masked clinicians categorised all RPA plots (progressing/not progressing), in addition to the measuring of significant RPA area. Masked OCT series assessment with linear regression of averaged global and sectoral cRNFL thickness was conducted as the 'clinical imaging standard'.

Main Outcome Measures

Inter-observer agreement was compared between RPA and the clinical imaging standard. Discriminative ability was assessed using receiver operating characteristic (ROC) curves. Time to detection of progression was compared using Kaplan-Meier survival analysis, and agreement of RPA with the clinical imaging standard was calculated.

Results

743 scans from 98 eyes were included in the study. Inter-observer agreement was significantly greater when categorising RPA (kappa = 0.86, 95% CI 0.81 – 0.91) compared to OCT image series (kappa = 0.66, 95% CI 0.54 – 0.77). The discriminative power of RPA to differentiate progressing from non-progressing eyes (AUC = 0.97, 95% CI 0.92 – 1.00) was greater than global cRNFL thickness (AUC = 0.71 95% CI 0.59 – 0.82, p<0.0001) and equivalent to sectoral cRNFL regression (AUC = 0.97, 95% CI 0.92 – 1.00). Kaplan-Meier survival analysis showed progression was detected 8.7 months sooner by RPA than global cRNFL linear regression (p<0.0001) in progressing eyes, however not compared with sectoral cRNFL (p=0.06). RPA showed substantial agreement with the presence of significant thinning on sectoral cRNFL linear regression (kappa=0.715, 95% CI 0.578-0.853).

Conclusions

RPA has been shown to provide accurate and intuitive at-a-glance data analysis and presentation that improves inter-observer agreement and may aid early diagnosis of glaucomatous disease progression.

Introduction

Retinal nerve fibre layer (RNFL) thickness is commonly used as a structural biomarker in the investigation of glaucoma patients. This parameter represents the health of the ganglion cell population from which the nerve fibres project. The speed and patient acceptability of optical coherence tomography (OCT) imaging has encouraged widespread, frequent use in disease monitoring, without harm to the patient. Thus, serial circumpapillary thickness measurements along a circular path around the optic nerve head complement functional outcomes (visual field testing) to inform clinicians on the stage, location and rate of ganglion cell loss, aiding diagnosis of glaucoma.

The thickness of the RNFL as measured by segmentation of cross-sectional OCT images has been shown to demonstrate reasonable discriminative and predictive abilities, often ahead of confirmed visual field loss[1,2]. However, the rate of disease progression is now routinely being used to individualise treatment in the context of existing glaucomatous damage, life expectancy, and comorbidities. The use of RNFL thinning to represent disease progression is evidenced by its association with worsening of visual field defects[3,4]. Therefore, it is paramount structural biomarkers are developed, enabling early detection of 'pre-perimetric' disease progression, and allowing timely instigation of therapy in order to prevent visual loss and blindness from end-stage disease[5].

'Progression analysis' of circumpapillary RNFL measures has been incorporated into the software of all major OCT platforms, with average rate of progression globally and sectorally assessed using linear regression over time. Although event-based analysis has been shown to possess equivalent accuracy[6], trend-based methods are less susceptible to anomalous results and are useful for extrapolating future field loss in the context of patient age. In contrast to visual field testing which can be limited by its subjective nature, a 'learning effect'[7], and poor reproducibility in the context of reduced visual acuity[8], OCT technology lends itself well to determining 'rate of progression' through

serial measures with excellent repeatability in the majority of cases[9]. Variation in optic disc and RNFL morphology can limit the diagnostic power of single scans relative to a normative database, whereas within-subject longitudinal assessment may be used to detect small amounts of structural change[10].

With diagnostic technologies generating ever-increasing amounts of data, efficiently summarising and communicating this information to facilitate clinical decision making requires the development of effective analysis and visualisation methods. Appropriate analysis harnesses the power of the data to its fullest extent, whilst intuitive data visualisation can better inform clinical decisions. Furthermore, the evolution of such clinical tools ensures adaptations are made in order to manage the increasing number of patients looked after worldwide[11]. We present the development of 'Rose Plot Analysis' (RPA), a novel method of circumpapillary RNFL (cRNFL) OCT data analysis and presentation that is able to comprehensively summarise the rate and location of structural progression 'at-a-glance'. The aim of this study is to investigate its effect on the reproducibility of clinical decision making and its potential for improving early diagnosis, using both qualitative and quantitative assessments of RNFL thickness through time to represent the current 'clinical imaging standard' of care.

Methods

RPA development

RPA was iteratively developed by a team of clinical ophthalmologists and scientific software developers. The unmet clinical need was described as 'at-a-glance' data presentation to comprehensively summarise the progression status of glaucomatous eyes. RPA displays a unique combination of information relating to an individual eye throughout the course of all visits, namely the rate, location and significance of RNFL thinning. These data are displayed in an angular histogram, and thus not summarised according to global or sectoral averages. Rate of thinning is represented by height of the graph, anatomical location of thinning is represented as the circumpapillary angular location on the angular histogram, and areas of thinning deemed to be significant are highlighted in red, according to the application of dynamic clustering (Figure 1).

Study participants

This study was given ethical approval by the Health Regulatory Authority of the United Kingdom (IRAS 282562). The study was carried out in accordance with the Declaration of Helsinki. Fully anonymised datasets were used for the purposes of this study. Consecutive eligible eyes were enrolled by clinicians from glaucoma clinics at the Western Eye Hospital, Imperial College Healthcare NHS Trust, London, UK. Eligible eyes were diagnosed or under observation for open-angle glaucoma with at least 5 referenced circumpapillary RNFL scans, and a minimum average global cRNFL of 50μm (to avoid the floor effect[12]). Eyes were excluded with significant media opacity, concomitant neurological or ocular disease were affecting optic nerve, retinal health or their morphology, or if extremes of refractive error (± 6 dioptres spherical equivalent or ± 3 dioptres of astigmatism) were present.

Imaging data

Images were acquired on the Spectralis spectral-domain imaging platform (SD-OCT, Heidelberg Engineering, Heidelberg, Germany). Built-in eye tracking and averaging processes were used to improve image quality. The in-built anatomical positioning system ensured accurate fovea-disc orientation throughout. Images were anatomically aligned between visits and the RNFL layer segmented automatically using the proprietary imaging software. Eyes were manually checked for imaging artefacts or segmentation errors and failure (including that caused by media opacity), and exclusions were made where present. No thresholding according to quality indicator was conducted to avoid selection bias. Raw numerical cRNFL data were extracted using a custom patch. This comprised of 768 A-scans from the 3.5mm diameter circumpapillary circle, centred on the optic nerve head at each visit, in addition to global and sectoral averages (according to 'Garway-Heath' sectors[13]). These data were imported into R (R Project for Statistical Computing[14]). Sectoral and global progression was calculated using ordinary least squares linear regression through time from baseline using R[14].

The RPA protocol was as follows; for each patient visit, data were aligned and presented as coordinate polar plots before ordinary least squares linear regression was performed at each of the 768 retinal layer thickness measurements through time (days), normalised to a baseline (first) visit. As regions of progression were expected to be larger than individual A-scans, resulting slopes were assessed for significant deviation from zero using a one-sample T-test (assessment for regions of thinning only) before resulting p-values were combined using a clustering by fast search method as previously described[15] (parameters δ=0.2, ρ=2.0). Assuming independence between resulting clusters, p-values were pooled using Fisher's method[16] and cluster progression was declared when $\alpha < 1x10^{-7}$ using the Holm-Bonferroni correction for multiple comparisons, with these regions presented in red. For the purpose of this study, data from each eye were evaluated independently.

Clinician OCT grading ('Clinical imaging standard')

To define the clinical imaging standard, OCT image series from study eyes were graded by three ophthalmologists (EN, PB, TY) independently, masked from any additional clinical information. The images available to the graders included cRNFL profiles plotted against the manufacturer's default normative database, with cRNFL thickness colour coded into green (within normal limits, $p>0.05$), amber (borderline, $p<0.05$) and red (outside normal limits, $p<0.01$), seven linear regression plots of averaged global and Garway-Heath sectoral cRNFL values through time, accompanied with the regression slope (μm/year) and statistical significance (p value). Eyes were graded by masked clinicians as 'progressing', 'stable', or 'unaffected', with the last two categories classed as 'non-progressing'. Progressing eyes were marked as 'progressing' if they would be placed under enhanced monitoring or treatment would be initiated/upgraded. The majority consensus ('progressing' or 'non-progressing') was used as the clinical imaging standard.

Quantitative OCT grading

Quantitative assessment of OCT series was carried out using ordinary least squares linear regression of cRNFL thickness through time (days). This was performed for the averaged global cRNFL measurement, and each of the 6 averaged 'Garway-Heath sector' cRNFL values (superotemporal, temporal, inferotemporal, inferonasal, nasal and superonasal) in the same manner as the proprietary progression analysis module. To simulate progression analysis completed at each visit for each eye through time, the regression of averaged global and sectoral RNFL thickness was carried out between each visit and baseline, incorporating the data acquired in between. For continuous variable analysis, the regression slope was used. For binary analysis ('progressing' or 'not progressing'), the presence of progression was defined as any series with statistically significant thinning ($p<0.05$).

Clinician RPA grading

All rose plots generated from RPA were graded independently by 3 ophthalmologists (EN, PB, TY) masked from any other imaging (including OCT scans) or further clinical information. Clinicians were asked to independently grade the plots as clinically 'progressing' or 'not progressing' after reviewing an SOP explaining the concepts of RPA displays. Plots were presented to the clinicians and graded in a custom program designed in R. The majority binary decision of three clinicians was taken as the qualitative clinician RPA categorisation.

Quantitative RPA grading

Rose plots were quantitatively assessed by measuring the total area of red (statistically significant cluster progression) in each plot, thus removing subjectivity and inter-observer variability. This continuous variable was calculated independently of the script used to generate the RPA plots, and quantified the area of red (in pixels) seen by the clinicians in each plot. Each plot was analysed using an ImageJ[17] macro to count red pixels.

Statistical analysis

Targeted analyses using the qualitative and quantitative gradings of both RPA and OCT imaging were carried out, each to investigate particular aspects of novel RPA methodology. These included inter-observer agreement to investigate reliability, receiver-operator characteristic (ROC) curves to compare discriminative ability against objective measures, time-to-event analysis to investigate the potential for early diagnosis, and 2-way tables to highlight agreement and safety (false negative rates).

Inter-observer agreement between three masked clinicians for both RPA and OCT series was assessed using Fleiss' kappa (κ) statistic. Agreement was regarded as 'none to slight' when between 0.01–0.20, 'fair' when 0.21–0.40, 'moderate' when 0.41– 0.60, 'substantial' when 0.61–0.80, and 'almost perfect' when 0.81–1.00[18,19].

ROC curves were used to compare the discriminative ability of objective RPA assessment (quantitative RPA grading) with objective OCT parameters (quantitative OCT grading), namely global cRNFL linear regression slope, and global cRNFL thickness at final visit. This was carried out using subjective and objective classifiers; the clinical imaging standard (clinician OCT categorisation) and the presence of statistically significant sectoral cRNFL linear regression. Area under the ROC curve (AUROC) of 0.5 was interpreted as discrimination equivalent to chance, and AUROC of 1 showing perfect discrimination. With a combination of parametric and non-parametric distributions of data, a parametric approach to ROC was maintained, as described previously[20]. DeLong's method was used to determine any significant differences between AUROCs[21]. Adjustment of p-values for multiple comparisons used the conservative Bonferroni method[22]. Quantitative RPA assessment (red area) was correlated with linear regression of cRNFL values. Correlation was termed 'strong' when the absolute value of r was greater than 0.7, 'moderate' when r was greater than 0.5, and 'weak' when greater than 0.3. All statistical analyses were carried out using R. ROC curves were plotted using ROCit[23].

Two-way tables were used to investigate the level of agreement of clinician RPA grading with three calssifiers; the clinical imaging standard (clinician OCT grading), and the presence or absence of a statistically significant negative trend ($p<0.05$) in global cRNFL, or any cRNFL sector using percentage agreement and Cohen's kappa (κ) statistic. Kaplan-Meier survival analysis was used as time-to-event analysis to simulate detection of progression through time in all eyes, and also just limited to those clinically labelled as 'progressing' by the clinical imaging standard. Time to detection of progression was compared between clinician RPA grading, versus the occurrence of a statistically significant linear trend ($p<0.05$) in global cRNFL, and the presence of a statistically significant linear trend ($p<0.05$) in any cRNFL sector. Statistical significance was declared when $p<0.05$ throughout.

289

Results

Study population

Seven hundred and forty-three scans from 98 eyes met the inclusion criteria for this study. The mean age of the patients (± SD) was 68.2 ± 12.0 years. 47% of patients were male, and 53% were female. 55% were right eyes and 45% left eyes. Mean starting visual field mean deviation (MD) was -4.0 ± 5.0 dB. Mean starting global average cRNFL was 79.1 ± 16.8 μm. The mean number of visits per eye was 7.6 ± 3.2 scans. These demographics and baseline statistics are separated into eyes classed as 'progressing' and 'not progressing' by the clinical imaging standard. There was a significantly thinner mean global cRNFL thickness in the 'progressing' group (p = <0.0001). There was no significant difference in starting MD between 'progressing' and 'not progressing' groups (p = 0.534). There was also no significant difference between the number of visits in each image series between groups (p=0.058) (Table 1).

Inter-observer agreement

The three-way agreement between the clinicians when categorising OCT series to form the clinical imaging standard was 83% (kappa 0.657, 0.542 – 0.771). Three-way agreement between the clinicians when categorising RPA was significantly greater at 90% (kappa 0.860, 95% CI 0.809 – 0.907) (Figure 2).

Discriminative ability of RPA

The ability of RPA to discriminate between OCT series categorised as 'progressing' and 'not progressing' by the clinical imaging standard was AUC = 0.97, 95% CI 0.92 – 1.00, significantly superior to that of global cRNFL thickness (AUC = 0.71 95% CI 0.59 – 0.83) (DeLong's method

p<0.0001), and comparable to linear regression of global cRNFL thickness (AUC = 0.97, 95% CI 0.92 – 1.00, p = 1.00) (Figure 3).

The ability of RPA to discriminate between OCT series categorised as 'progressing' and 'not progressing' by the presence of any significant sectoral cRNFL thinning was (AUC = 0.95, 95% CI 0.90 – 0.99), significantly superior to that of global cRNFL thickness (AUC = 0.61, 95% CI 0.50 – 0.73, p<0.0001), and comparable to linear regression of global cRNFL thickness (AUC = 0.94, 95% CI 0.89 – 0.99, p = 1.00) (Figure 3).

Agreement of RPA with the clinical imaging standard

Agreement of clinician RPA categorisation with the clinical imaging standard was 77.6% (kappa 0.555, 95% CI 0.389-0.721). In all eyes where there was disagreement, RPA was categorised as 'progressing', whilst the clinical imaging standard categorised them as 'not progressing' (Appendix 3).

Agreement of RPA with linear regression of OCT data

Agreement of clinician RPA categorisation with the presence of a statistically significant trend in *global* cRNFL thinning was 68.4% (kappa 0.375, 95% CI 0.165-0.585). In all eyes where there was disagreement, RPA was categorised as 'progressing' whilst the clinical imaging standard categorised them as 'not progressing' (Appendix 3).

Agreement of clinician RPA categorisation with the presence of a statistically significant trend in *sectoral* cRNFL thinning was 85.7% (kappa 0.715, 95% CI 0.578-0.853). In the eyes where there was disagreement, 11.2% of eyes were marked as progressing with RPA, and 3% marked as progressing with linear regression of sectoral cRNFL (Appendix 3). Examples of RPA plots that were in agreement and disagreement with the clinical imaging standard are displayed in Appendix 1.

Correlation of RPA with linear regression

RPA red area was significantly different between those graded as progressing and non-progressing with the clinical imaging standard ($p<0.0001$, n=743). There was a strong positive correlation between RPA red area and rate of *global* cRNFL thinning in eyes categorised as 'progressing' by the clinical imaging standard ($r = 0.930$, $R^2 = 0.865$, $p <0.0001$). To a much lesser extent, a weak correlation was present with the eyes labelled 'non-progressing' by the clinical imaging standard ($r = 0.415$, $R^2 = 0.172$, $p <0.001$). There was a strong positive correlation between RPA red area and rate of *sectoral* cRNFL thinning (fastest progressing sector) in eyes both categorised as 'progressing' ($r = 0.730$, $R^2 = 0.533$, $p <0.0001$) and 'non-progressing' ($r = 0.738$, $R^2 = 0.545$, $p <0.0001$) by the clinical imaging standard (Appendix 2).

Survival analysis

Kaplan-Meier survival analysis revealed statistically significant earlier detection of progression using clinician RPA categorisation compared to the presence of significant thinning of global cRNFL using linear regression.

Amongst *all* patients at the end of year 1, 10% were marked progressing with global cRNFL linear regression and 41% with RPA, and at the end of year 2, 56% with global cRNFL and 78% with RPA ($p<0.0001$ overall). Median survival was greater than 912 days (95% CI 883 – >912) with global cRNFL, and 511 days (95% CI 378 – 699) with RPA, a reduction of at least 401 days ($p<0.0001$). Exclusively amongst those eyes categorised as 'progressing' by the clinical imaging standard, 21% were marked progressing with global cRNFL and 71% with RPA at the end of year 1, and 79% with global cRNFL and 96% with RPA at the end of year 2. Median survival was 527 days (95% CI 456 –

598) with global cRNFL, and 263 days (95% CI 182 – 365) with RPA, a reduction of 264 days (p <0.0001) (Figure 4).

Amongst *all* patients at the end of year 1, 32% were marked progressing with sectoral cRNFL linear regression (any sector) compared to 41% with RPA, and at the end of year 2, 73% with sectoral cRNFL compared to 78% with RPA. Median survival with sectoral cRNFL was 699 days (95% CI 502-875), and 511 days (95% CI 378-699) with RPA (p = 0.064). Amongst patients categorised as 'progressing' at by the clinical imaging standard, 61% were marked progressing with sectoral cRNFL compared with 71% with RPA at the end of year 1, and 93% with sectoral cRNFL compared to 96% with RPA at the end of year 2. Median survival was 306 days (95% CI 239-462) with sectoral cRNFL, and 262 days (95% CI 182-365) with RPA (p = 0.270) (Figure 4).

Discussion

This study has demonstrated RPA as a novel analysis and visualisation tool that is able to accurately and intuitively display comprehensive structural progression data. Incorporated in the output are the rate, location, and significance of RNFL thinning, creating a powerful 'at-a-glance' plot that is anatomically orientated and easily interpretable. This study has demonstrated that RPA can improve agreement between clinicians and potentially assist in the early diagnosis of glaucoma progression.

The imperfect agreement between clinical endpoints when detecting glaucoma progression has previously been demonstrated[24]. Furthermore, poor inter-observer agreement plagues reproducibility of clinical decisions and equality in standards of care[25-27]. When assessing optic disc photographs and standard automated perimetry, inter-rater kappa has been quoted as 0.16 and 0.13 respectively[26]. Although OCT has been shown to accurately and consistently detect pre-existing glaucomatous damage[26], refinement of progression analysis is required to differentiate those with progressive disease requiring more aggressive treatment. The use of objective progression analysis to aid assessment of change between visits has been demonstrated in visual field testing[28]. However, the OCT equivalent using linear regression confined to predefined circumpapillary sectors is time-consuming to review, and increases the potential for inter-observer variability. Consequently, the lack of an agreed systematic approach results in clinicians giving varying degrees of importance to biomarkers when assessing patients. Hood et al. suggested a single-page display of OCT data to guide systematic assessment for structural damage, also aiding correlation to functional data[29]. In a similar manner, our study demonstrates that RPA can act as a decision-making tool for progression analysis. The improved inter-observer agreement promises great potential to provide better consistency and standardisation of treatment decisions, with RPA displaying circumferential progression data in a single circular plot. Furthermore, due to the ease with which the results can be anatomically correlated, the plot is a compelling qualitative and quantitative novel assessment tool.

The widespread uptake of structural imaging is believed to have increased diagnostic sensitivity for glaucoma, with many OCT studies differentiating glaucomatous from healthy eyes. A recent meta-analysis[1] reported a pooled AUROC of 0.897 (95% CI 0.887 – 0.906) for circumpapillary RNFL measures. However, stratifying eyes in such a way does not confer the rate of progression, whereas the clinical objective is often to highlight those in most need of urgent treatment. Thus, plotting a dynamic process such as in RPA has more important implications on the future trajectory of the patient's visual status and the immediate need for treatment. In the evolution of visual field progression analysis, event-based and trend-based approaches have been compared, with the results demonstrating similar performance between the two methods[30]. Similar comparisons of progression analysis methodology have been made for OCT imaging, with some superiority of the trend-based approach adopted in RPA[31] reported. In further developing trend-based approaches, pointwise linear regression in visual field testing increased the resolution of analysis in comparison to regression of summary measures[32,33], and in analogous fashion, pointwise linear regression of circumpapillary thickness points has been built into RPA with the aim of identifying earlier structural changes.

The use of angular histograms in glaucoma progression is a novel application in the field of medical imaging. However, the plots have been successfully applied in other fields, namely meteorology[34]. The unique ability to plot vectors in a circumferential manner conveys both magnitude and spatial information for applications such as wind speed and direction, where both may be critically important. In the case of glaucoma, it is characteristically the supertemporal and inferotemporal nerve fibre bundles that appear particularly vulnerable to damage and thus may be differentiated from other patterns of nerve fibre loss[29].

In contrast to averaged circumpapillary sectors commonly used in clinical practice,[13] the variable sector size of RPA allows intelligent multi-dimensional rose formation whilst giving more statistical weight to clusters of progressing circumpapillary points. Not only does this function as effective noise-filtration, but also is likely to allow for a greater range of developing RNFL defect sizes to be highlighted[35]. For instance, small discrete bundles of nerve fibres can often display subtle thinning in

early disease[36], that may not be of sufficient size to influence summary values based on sectoral or global averages. The multi-dimensional intelligence of RPA displays has the potential for yet further expansion by incorporating multiple circle scan diameters in transparent rose plots to emphasise thinning at multiple circumpapillary diameter. Thus, the improved granularity of RPA is in keeping with better diagnostic sensitivity, avoiding the pitfalls of diagnosing 'red' and 'green' disease when summary measures are taken at face value[37]. This theory is matched by the results of this study, demonstrating significantly reduced time to detect progression using RPA compared to the global RNFL linear regression (and near significance with the sectoral indices). The excellent results in terms of sensitivity (very few cases where RPA did not detect progression labelled by other methods), when compared with regression indices mean that RPA is a safe tool in reassuring clinicians of the absence of progression, potentially helping over-burdened services[38].

Limitations of this study include the exclusion of functional outcomes, whilst instead comparing with a clinical imaging standard that is used as structural information as part of the patient assessment. The exact relationship between structure and function assessed with the biomarkers available is complex and continues to be fully characterised[39,40] and therefore, the challenge in glaucoma research remains finding a 'gold standard' allowing full adherence to the recommended STARD (Standards for Reporting of Diagnostic Accuracy Studies) guidelines[41,42] for diagnostic accuracy studies. It is critical that studies of any new assessment of the clinical utility of a new diagnostic technique follows such guidelines; our study was not designed in this way. In order to link the earliest changes observed on RPA with functional loss, longitudinal prospective studies with regular visual field monitoring would be required. Within this, recruitment could be stratified by baseline disease severity in order to ascertain the effect on RPA sensitivity as the minimum cRNFL 'floor' thickness is approached[12], and conversely to exclusively examine 'pre-perimetric' patients, where RPA has the greatest potential to improve early diagnosis. Prior work associating points of visual field loss with circumpapillary structural locations[29] may then be used to incorporate existing functional losses on the rose plots or even predict vulnerable points on the visual field [40].

The future of structural biomarkers in glaucoma may lie in developing discerning combinations of multi-modal imaging specifically tailored to the clinical task at hand, for clinicians appropriately qualified to interpret the data in the context of the whole patient. Increasing attention is being given to glaucoma as a retinal disease, with posterior pole scanning protocols providing glaucoma diagnosis with AUROC of 0.885 (95% CI 0.869 to 0.901) for the macular ganglion cell complex, along with mapping of structural changes to functional losses in other novel methods of data presentation[43]. Trend-based progression analyses using these data are still to be refined. However, to utilise historical circumpapillary RNFL data, RPA is well-placed to 'signpost' attention to particular regions of interest that can be extrapolated to examination findings and other investigations in keeping with topographical structure-functional relationships[44]. With our results demonstrating the multi-faceted potential that RPA has in clinical glaucoma care, we propose its clinical introduction as a structural representative incorporated into the comprehensive patient assessment in order to improve clinical decision making and the care of our patients.

References

1. Kansal V, Armstrong JJ, Pintwala R, Hutnik C. Optical coherence tomography for glaucoma diagnosis: An evidence based meta-analysis. *PLoS One.* 2018;13(1):e0190621.
2. Lalezary M, Medeiros FA, Weinreb RN, et al. Baseline optical coherence tomography predicts the development of glaucomatous change in glaucoma suspects. *Am J Ophthalmol.* 2006;142(4):576-582.
3. Miki A, Medeiros FA, Weinreb RN, et al. Rates of retinal nerve fiber layer thinning in glaucoma suspect eyes. *Ophthalmology.* 2014;121(7):1350-1358.
4. Tatham AJ, Medeiros FA. Detecting Structural Progression in Glaucoma with Optical Coherence Tomography. *Ophthalmology.* 2017;124(12S):S57-S65.
5. Susanna R, Jr., De Moraes CG, Cioffi GA, Ritch R. Why Do People (Still) Go Blind from Glaucoma? *Transl Vis Sci Technol.* 2015;4(2):1.
6. Yu M, Lin C, Weinreb RN, Lai G, Chiu V, Leung CK. Risk of Visual Field Progression in Glaucoma Patients with Progressive Retinal Nerve Fiber Layer Thinning: A 5-Year Prospective Study. *Ophthalmology.* 2016;123(6):1201-1210.
7. Chauhan BC, Garway-Heath DF, Goni FJ, et al. Practical recommendations for measuring rates of visual field change in glaucoma. *Br J Ophthalmol.* 2008;92(4):569-573.
8. Matsuura M, Hirasawa K, Murata H, Asaoka R. The Relationship Between Visual Acuity and the Reproducibility of Visual Field Measurements in Glaucoma Patients. *Invest Ophthalmol Vis Sci.* 2015;56(9):5630-5635.
9. Toteberg-Harms M, Sturm V, Knecht PB, Funk J, Menke MN. Repeatability of nerve fiber layer thickness measurements in patients with glaucoma and without glaucoma using spectral-domain and time-domain OCT. *Graefes Arch Clin Exp Ophthalmol.* 2012;250(2):279-287.
10. Zhang X, Dastiridou A, Francis BA, et al. Comparison of Glaucoma Progression Detection by Optical Coherence Tomography and Visual Field. *Am J Ophthalmol.* 2017;184:63-74.
11. Tham YC, Li X, Wong TY, Quigley HA, Aung T, Cheng CY. Global prevalence of glaucoma and projections of glaucoma burden through 2040: a systematic review and meta-analysis. *Ophthalmology.* 2014;121(11):2081-2090.
12. Bowd C, Zangwill LM, Weinreb RN, Medeiros FA, Belghith A. Estimating Optical Coherence Tomography Structural Measurement Floors to Improve Detection of Progression in Advanced Glaucoma. *Am J Ophthalmol.* 2017;175:37-44.
13. Garway-Heath DF, Poinoosawmy D, Fitzke FW, Hitchings RA. Mapping the visual field to the optic disc in normal tension glaucoma eyes. *Ophthalmology.* 2000;107(10):1809-1815.
14. RStudio Team (2015) R, Inc., Boston, MA. RStudio: Integrated Development for R.
15. Rodriguez A, Laio A. Machine learning. Clustering by fast search and find of density peaks. *Science.* 2014;344(6191):1492-1496.
16. Owen AB. Karl Pearson's meta-analysis revisited. *The Institute of Mathematical Statistics.* 2009;37(6B):3867--3892.
17. Schneider CA, Rasband WS, Eliceiri KW. NIH Image to ImageJ: 25 years of image analysis. *Nat Methods.* 2012;9(7):671-675.
18. Cohen J. A coefficient of agreement for nominal scales. *Educational and psychological measurement.* 1960;20(1):37-46.
19. McHugh ML. Interrater reliability: the kappa statistic. *Biochem Med (Zagreb).* 2012;22(3):276-282.
20. Hajian-Tilaki KO, Hanley JA, Joseph L, Collet J-P. A comparison of parametric and nonparametric approaches to ROC analysis of quantitative diagnostic tests. *Medical Decision Making.* 1997;17(1):94-102.
21. DeLong ER, DeLong DM, Clarke-Pearson DL. Comparing the areas under two or more correlated receiver operating characteristic curves: a nonparametric approach. *Biometrics.* 1988;44(3):837-845.
22. Dunn OJ. Multiple Comparisons among Means. *Journal of the American Statistical Association.* 1961;56(293):52-64.

23. ROCit. https://CRAN.R-project.org/package=ROCit Accessed.
24. Banegas SA, Anton A, Morilla-Grasa A, Bogado M, Ayala EM, Moreno-Montanes J. Agreement among spectral-domain optical coherence tomography, standard automated perimetry, and stereophotography in the detection of glaucoma progression. *Invest Ophthalmol Vis Sci.* 2015;56(2):1253-1260.
25. Moreno-Montanes J, Anton V, Anton A, et al. Intraobserver and Interobserver Agreement of Structural and Functional Software Programs for Measuring Glaucoma Progression. *JAMA Ophthalmol.* 2017;135(4):313-319.
26. Blumberg DM, De Moraes CG, Liebmann JM, et al. Technology and the Glaucoma Suspect. *Invest Ophthalmol Vis Sci.* 2016;57(9):OCT80-85.
27. Viswanathan AC, Crabb DP, McNaught AI, et al. Interobserver agreement on visual field progression in glaucoma: a comparison of methods. *Br J Ophthalmol.* 2003;87(6):726-730.
28. Nouri-Mahdavi K, Hoffman D, Ralli M, Caprioli J. Comparison of methods to predict visual field progression in glaucoma. *Arch Ophthalmol.* 2007;125(9):1176-1181.
29. Hood DC. Improving our understanding, and detection, of glaucomatous damage: An approach based upon optical coherence tomography (OCT). *Prog Retin Eye Res.* 2017;57:46-75.
30. Wu Z, Medeiros FA. Comparison of Visual Field Point-Wise Event-Based and Global Trend-Based Analysis for Detecting Glaucomatous Progression. *Transl Vis Sci Technol.* 2018;7(4):20.
31. Leung CK-S, Lin C, Yu M. Trend-based Progression Analysis (TPA): A New Algorithm for Visualizing the Topology of Progressive Retinal Nerve Fiber Layer (RNFL) Thinning in Glaucoma. *Investigative Ophthalmology & Visual Science.* 2015;56(7):3980-3980.
32. Fitzke FW, Hitchings RA, Poinoosawmy D, McNaught AI, Crabb DP. Analysis of visual field progression in glaucoma. *Br J Ophthalmol.* 1996;80(1):40-48.
33. O'Leary N, Chauhan BC, Artes PH. Visual field progression in glaucoma: estimating the overall significance of deterioration with permutation analyses of pointwise linear regression (PoPLR). *Invest Ophthalmol Vis Sci.* 2012;53(11):6776-6784.
34. Droppo JG, Napier BA. Wind direction bias in generating wind roses and conducting sector-based air dispersion modeling. *J Air Waste Manag Assoc.* 2008;58(7):913-918.
35. Leung CK, Mohamed S, Leung KS, et al. Retinal nerve fiber layer measurements in myopia: An optical coherence tomography study. *Invest Ophthalmol Vis Sci.* 2006;47(12):5171-5176.
36. Jonas JB, Schiro D. Localised wedge shaped defects of the retinal nerve fibre layer in glaucoma. *Br J Ophthalmol.* 1994;78(4):285-290.
37. Chong GT, Lee RK. Glaucoma versus red disease: imaging and glaucoma diagnosis. *Curr Opin Ophthalmol.* 2012;23(2):79-88.
38. Morley AM, Murdoch I. The future of glaucoma clinics. *Br J Ophthalmol.* 2006;90(5):640-645.
39. Zhu H, Crabb DP, Fredette MJ, Anderson DR, Garway-Heath DF. Quantifying discordance between structure and function measurements in the clinical assessment of glaucoma. *Arch Ophthalmol.* 2011;129(9):1167-1174.
40. Kihara Y, Montesano G, Chen A, et al. Policy-Driven, Multimodal Deep Learning for Predicting Visual Fields from the Optic Disc and OCT Imaging. *Ophthalmology.* 2022.
41. Cohen JF, Korevaar DA, Altman DG, et al. STARD 2015 guidelines for reporting diagnostic accuracy studies: explanation and elaboration. *BMJ Open.* 2016;6(11):e012799.
42. Fidalgo BM, Crabb DP, Lawrenson JG. Methodology and reporting of diagnostic accuracy studies of automated perimetry in glaucoma: evaluation using a standardised approach. *Ophthalmic Physiol Opt.* 2015;35(3):315-323.
43. Hood DC, Raza AS, De Moraes CG, et al. Evaluation of a One-Page Report to Aid in Detecting Glaucomatous Damage. *Transl Vis Sci Technol.* 2014;3(6):8.
44. Ferreras A, Pablo LE, Garway-Heath DF, Fogagnolo P, Garcia-Feijoo J. Mapping standard automated perimetry to the peripapillary retinal nerve fiber layer in glaucoma. *Invest Ophthalmol Vis Sci.* 2008;49(7):3018-3025.

Legends

Figure 1. Examples of RPA plots from two patients. RPA uses centripetal height of the graph to show rate of thinning, the circumferential position to show circumpapillary location of thinning, and colour of the graph to show statistical significance, in a single 'at-a-glance' plot. Top row: A patient with a significantly progressing right eye and stable left eye. Bottom row: A patient with a progressing right eye, and a left eye with progression only highlighted using RPA. 'Garway-Heath' sectors are included centrally for anatomical orientation. R = right eye, L = left eye, TS = superotemporal, NS = superonasal, N = nasal, NI = inferonasal, TI = inferotemporal, T = temporal. Further examples are shown in Appendix 1.

Table 1. Baseline characteristics of eyes included in the study. The data has also been subdivided into those eyes categorised as 'progressing' and 'not progressing' by the clinical imaging standard (masked clinician assessment of OCT series).

Figure 2. Comparison of masked clinician inter-observer agreement assessing Rose Plot Analysis (RPA) and OCT series (clinical imaging standard). RPA demonstrated significantly greater agreement (Fleiss' kappa 0.86, 95% CI 0.81 – 0.91 vs 0.66, 95% CI 0.54 – 0.77) when assessed for disease progression.

Figure 3. Receiver-operating characteristic curves showing the ability RPA (red area), the rate of global cRNFL thinning, and mean global cRNFL thickness (latest) to discriminate between eyes with 'progressing' and 'non-progressing' disease. Area under the curve (AUROC, 95% CI) is shown for each plot. Eyes were classified as 'progressing' and 'non-progressing' by two methods. Upper row: clinician assessment of OCT series – clinical imaging standard. Bottom row: the presence of at least one circumpapillary sector demonstrating significant thinning using linear regression. A significant

627 difference was found between the AUROCs of gRNFL thickness and both RPA and global cRNFL
628 regression in the case of both classifiers (DeLong's method, adjusted p-value < 0.0001).
629
630 **Figure 4.** Kaplan-Meier survival curves comparing the detection of progression using RPA (green)
631 and linear regression (red) in the same eyes with time (1 event = detection of progression). Majority
632 clinician assessment of RPA was compared against two other markers: the presence of global and
633 sectoral cRNFL statistically significant thinning on linear regression. This was examined in two
634 cohorts: in all study eyes (top row), and in those graded as 'progressing' by the clinical imaging
635 standard (bottom row). Statistically significant improvements were seen with RPA vs the global
636 cRNFL thinning in both cohorts (Median survival, all eyes: LinReg G >912.5 days (95% CI 883 –
637 >912.5), RPA 511 days (95% CI 378 – 699) (p<0.0001), 'Progressing' only: LinReg G 527 days
638 (95% CI 456 – 598), RPA 263 days (95% CI 182 – 365), (p <0.0001)), but not compared to sectoral
639 cRNFL thinning (Median survival, all eyes: LinReg S 699 days (95% CI 502-875), RPA 511 days
640 (95% CI 378-699) (p = 0.064), "Progressing" only: LinReg S 306 days (95% CI 239-462), RPA 262
641 days (95% CI 182-365) (p = 0.270)). LinReg G – Linear regression of global cRNFL, LinReg S –
642 Linear regression of sectoral cRNFL.
643
644

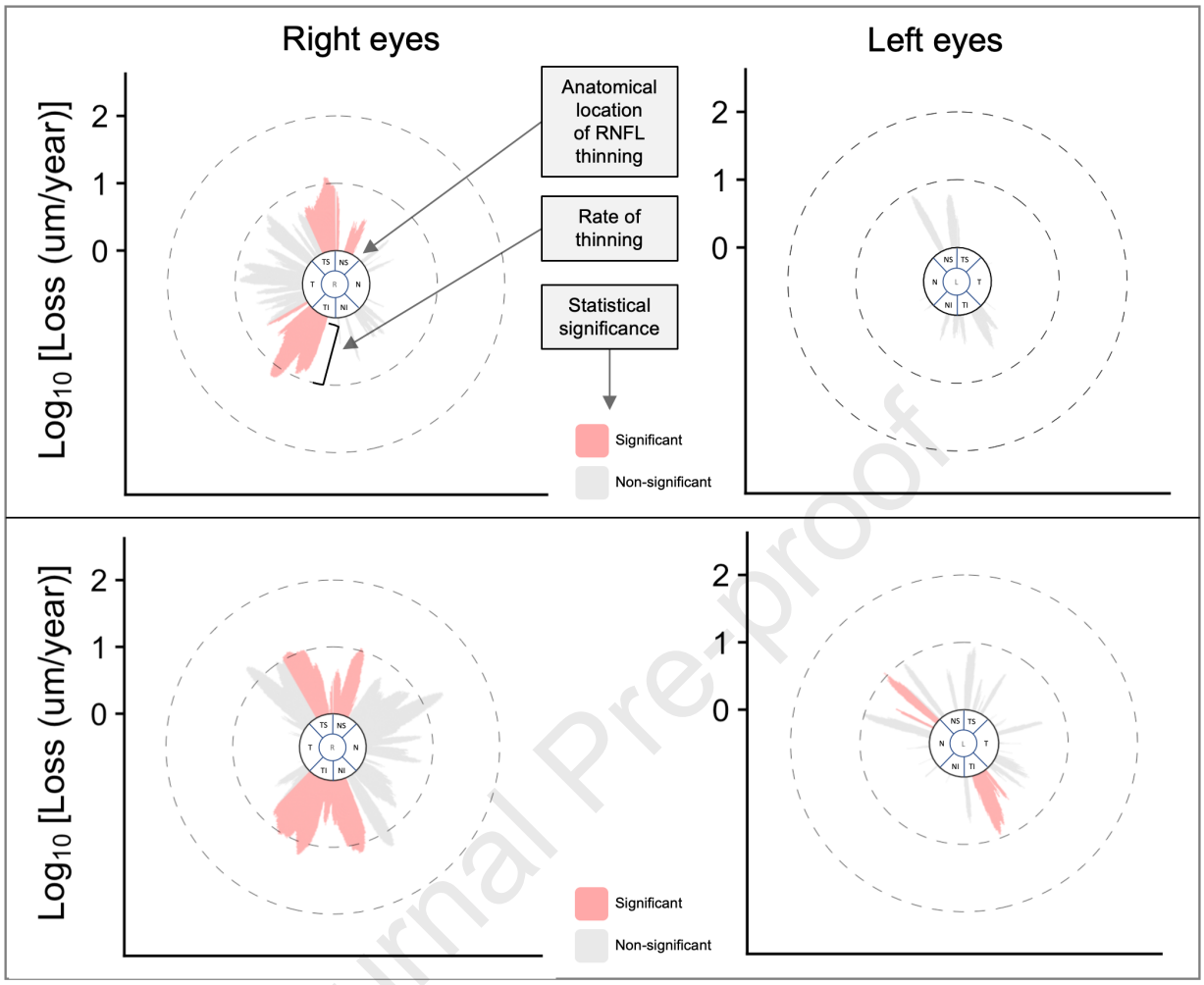

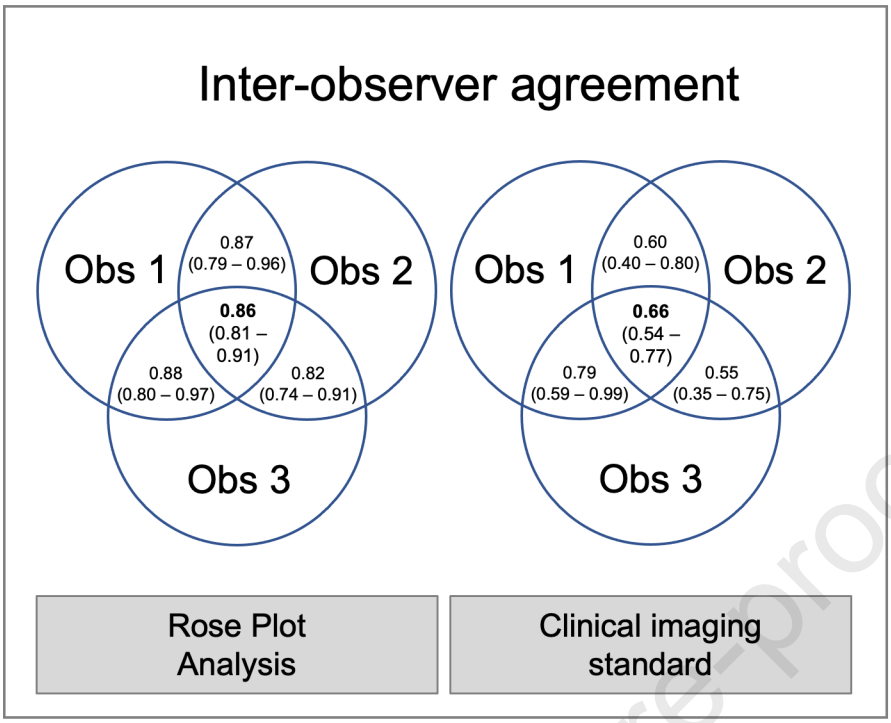

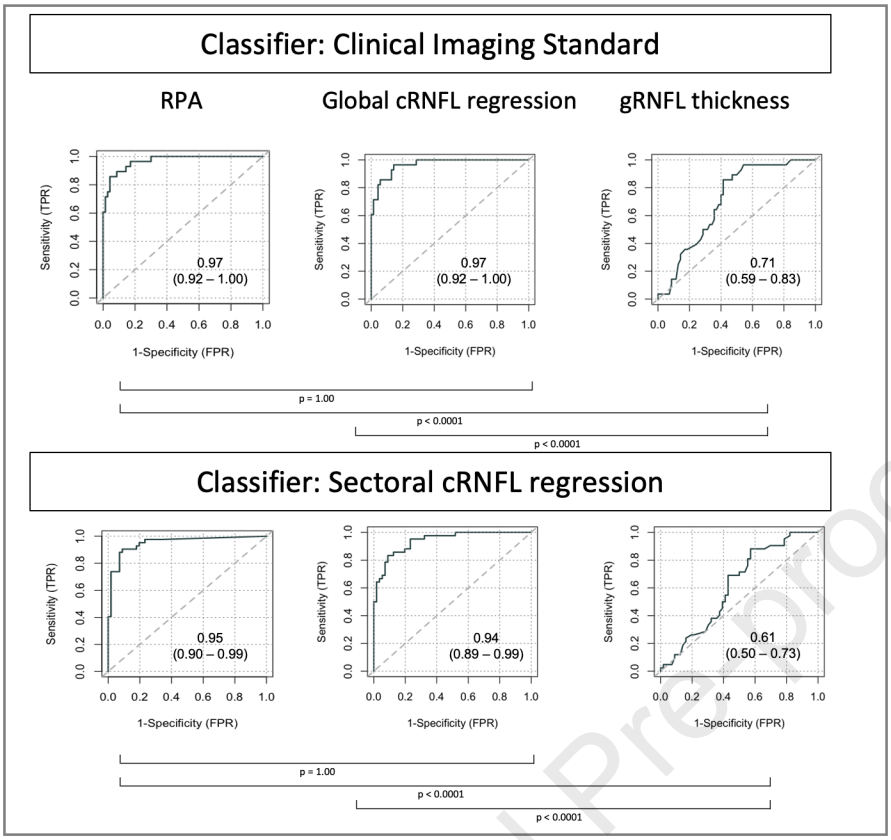

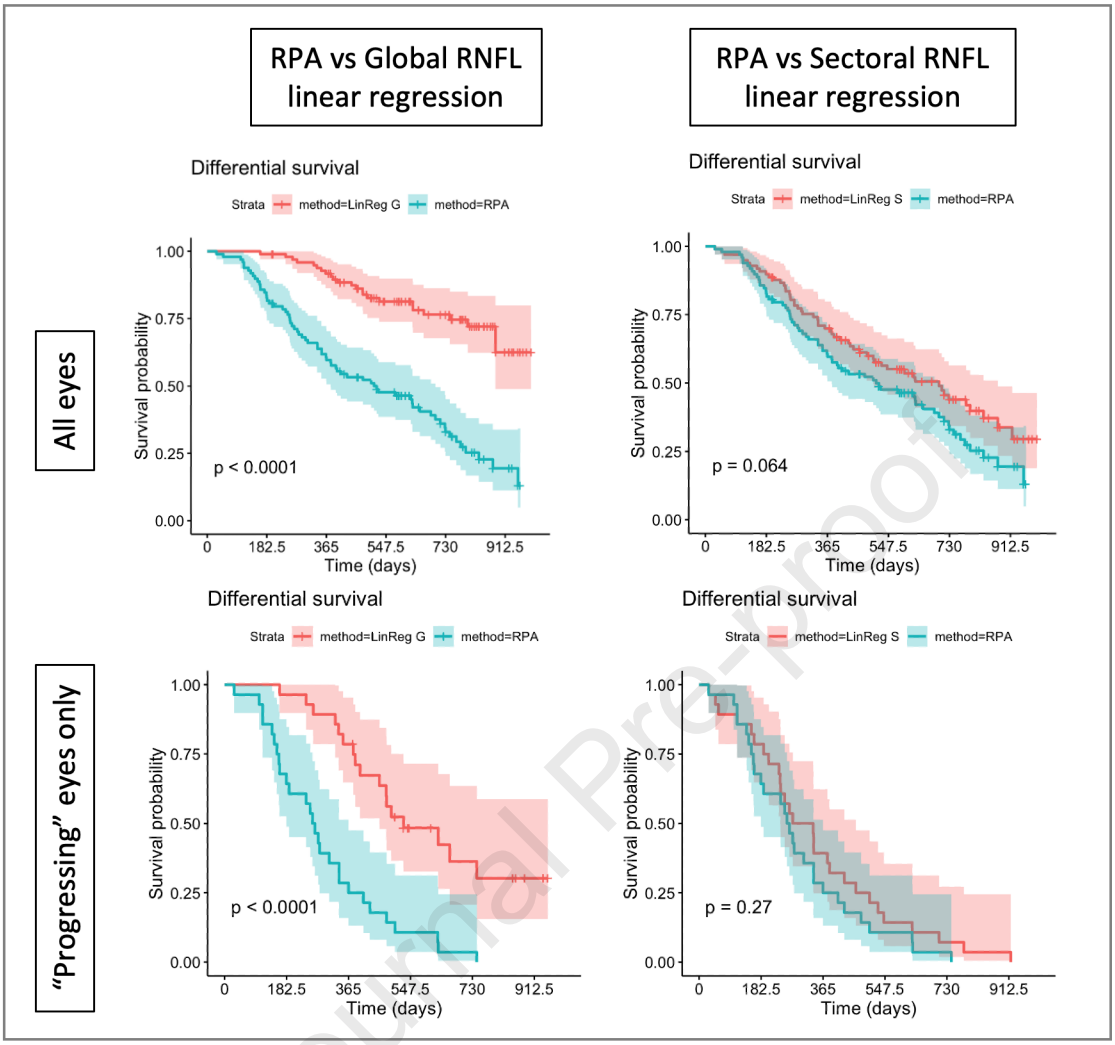

Patient Characteristics				
	Overall	"Progressing"	"Not progressing"	p
Patients, n	**91**	25	66	-
Eyes, n	**98**	28	70	-
Mean age ± SD, years	**67.8 ± 12.3**	65.4 ± 11.6	68.7 ± 12.5	0.255
Gender, M:F %	**47% : 53%**	52% : 48%	45% : 55%	0.396
Laterality (OD : OS)	**55% : 45%**	48% : 52%	57% : 43%	0.257
Starting MD ± SD, dB	**-4.0 ± 5.0**	-4.5 ± 4.5	-3.8 ± 5.2	0.534
Starting global cRNFL thickness ± SD, µm	**79.1 ± 16.8**	74.3 ± 11.7	81.1 ± 18.2	**<0.0001**
Mean number of visits ± SD, n	**7.5 ± 3.2**	8.5 ± 3.8	7.1 ± 2.8	0.058

Table 1. Baseline characteristics of eyes included in the study. The data has also been subdivided into those eyes categorised as 'progressing' and 'not progressing' by the clinical standard (masked clinician assessment of OCT series).

		RPA (consensus)		
		Stable	Prog	
CLINICAL STANDARD	Stable	48	22	70
	Prog	0	28	28
		48	50	98

Agreement	77.6%
kappa	0.555
kappa se	0.085
kappa lower	0.389
kappa upper	0.721

		RPA (consensus)		
		Stable	Prog	
Global cRNFL prog	Stable	48	31	79
	Prog	0	19	19
		48	50	98

Agreement	68.4%
kappa	0.375
kappa se	0.107
kappa lower	0.165
kappa upper	0.585

		RPA (consensus)		
		Stable	Prog	
Sectoral cRNFL prog	Stable	45	11	56
	Prog	3	39	42
		48	50	98

Agreement	85.7%
kappa	0.715
kappa se	0.070
kappa lower	0.578
kappa upper	0.853

Table 2. Two-way tables demonstrating agreement of masked RPA assessments with a) the clinical standard (clinician OCT series assessment) b) the presence of global or c) sectoral cRNFL thinning with linear regression.

Glaucoma Rose Plots are a novel progression analysis tool displaying circumpapillary OCT progression in a single at-a-glance plot. Their use improves inter-observer agreement on progression and detects progression faster than the current clinical standard.